Tomographic methods for magnetospheric applications

H. U. Frey, S. Frey, D. Larson

Space Sciences Laboratory, University of California, Berkeley, CA 94720-7450, U.S.A.

T. Nygrén

Department of Physical Sciences, University of Oulu, FIN-90570 Oulu, Finland

J. Semeter

Max-Planck-Institute for Extraterrestrial Physics, D-85740 Garching, Germany

Abstract. The mathematics of tomography was developed for medical applications when the patient may be examined under controlled circumstances. Geophysical applications can generally not meet this situation and result in erratic or impossible reconstructions if minimum requirements are not fulfilled.
This paper summarizes several tomographic reconstruction methods and shows the limitations and minimum requirements for magnetospheric applications. The reconstruction of a simple phantom is used as a point of comparison for the various methods. Under experimental conditions with a very limited angular range and a small number of observers, algebraic and statistical reconstruction methods generally yield better results than transform techniques.

1. Introduction

The aim of tomography is to reconstruct an unknown n-dimensional source distribution from a set of (n-1)-dimensional remote measurements. In the mathematical sense it is an inverse problem [*Natterer,* 1986]. The best known application is in medical diagnosis whereby images of the interior of the body are reconstructed from a set of X-ray projections.

Tomography in geophysics has long been used for the reconstruction of geological structures [*Menke,* 1984 and references therein] but just recently it has found applications in ionospheric research. Ionospheric tomography reconstructs the electron density distribution in an altitude-latitude plane from satellite measurements of the total ionospheric electron content [*Raymund et al.,* 1995]. These measurements assume spatial homogeneity in longitude and temporal stationarity. Thus, temporal fluctuations can not be studied with this method, and satellite passes need not necessarily coincide with interesting events. Nevertheless, this method achieved highly desired gross-scale results in large polar regions and radars provided fundamental independent data used for the verification of ionospheric reconstructions [*Walker et al.,* 1996; *Nygrén et al.,* 1996].

Scanning photometers and cameras can be used in a similar way to obtain two-dimensional [*Aso et al.,* 1990; *Vallance Jones et al.,* 1991; *Doe et al.,* 1997] or three-dimensional auroral volume emission reconstructions [*Frey et al.,* 1996; 1998]. As in general geophysical tomography, auroral tomography with ground-based optical instruments is restricted to a small number of cameras within a limited angular range. Proper reconstruction methods have to account for these limitations.

The aim of this paper is to summarize different reconstruction techniques which have been used in ionospheric research and compare the results for magnetospheric reconstructions from radio sounding measurements. This comparison is made with a phantom plane of electron density distributions. Even a carefully-designed multi-satellite mission cannot guarantee tomographic measurements from a complete set of angles around the object. An important point of comparison, therefore, is the sensitivity of the various techniques to incomplete data.

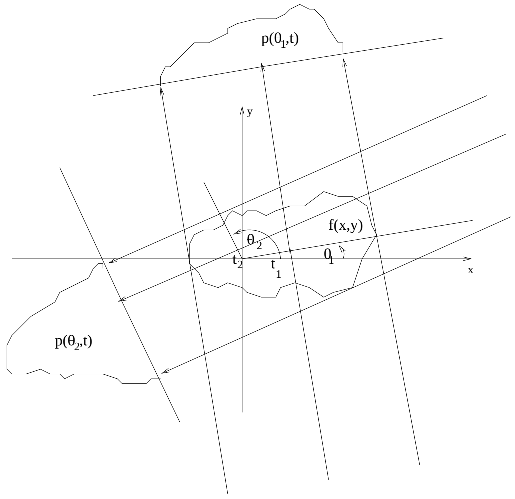

Figure 1. Parallel beam geometry.

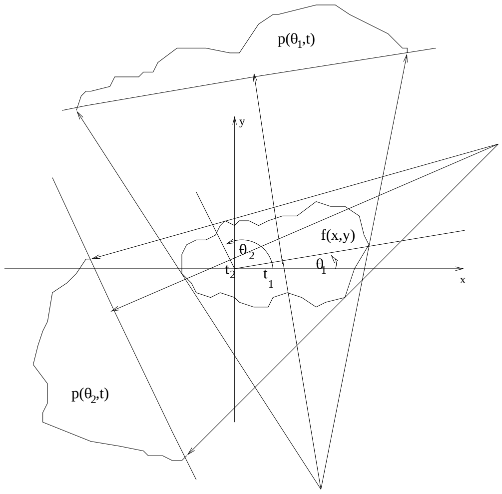

Figure 2. Fan beam geometry.

2. Tomographic methods

2.1. Remote measurements

Many investigations determine the integral of some property along lines from the observer position at $\mathbf{r} = 0$ through the object as the projection $p_i(\theta, \phi, t)$

$$p_i(\theta, \phi, t) = C \int_0^{\infty} f(\mathbf{r}(l)) \exp\left\{ - \int_{s=0}^{s=l} \mu(s) ds \right\} \mathrm{d}l \qquad (1)$$

with the source distribution $f(\mathbf{r})$ and a general absorption term $\mu(s)$. The unknown quantity is either the source distribution, or the distribution of the absorbing matter, or both. Computed tomography is then used to determine the distribution of the unknown quantity from a set of line integral measurements.

In the computerized discrete case, the plane is divided into small pixel, with the value in each pixel (x, y) representing the mean of the source distribution $f(x, y)$. For the purpose of better visualization the following presentation shows the reconstruction of a 2D-distribution, but in general it can also be used for 3D problems.

The parameter C contains measurement parameters. In this investigation we want to approximate the absorption as constant and (1) simplifies to

$$p_i(\theta, t) \approx C' \sum_{x,y} h_{xy}^{i\theta t} f(x, y) \qquad (2)$$

with $h_{xy}^{i\theta t}$ describing the contribution of the pixel (x,y) to the region subtended by the ray for the observer i.

The measurement geometries are based on parallel (Figure 1) or diverging fan (Figure 2) beams. Diffracting media need full angular coverage around the object. However, for non-diffracting media parallel projections which are 180° apart are just redundant mirror images of each other [*Kak and Slaney,* 1988], and it is sufficient to measure projections for angles from 180°. For measurements with a fan-beam angle of γ projections in an angular region of

$$\theta_0 \leq \theta < \theta_0 + 180^\circ + 2\gamma \qquad (3)$$

are necessary. Even this angular range can not be provided in most geophysical applications which leads to the so-called missing cone problem [*Hayner and Jenkins,* 1984]. One further characteristics of geophysical applications is that the objects are generally smooth with features of similar contrast and there are no sharp borders like bones in medical tomography.

The goal of tomography is to solve the set of linear equations (2). Various methods have been developed to find an estimate $\hat{f}$ of f [for reviews, see e.g., *Budinger and Gullberg,* 1974; *Natterer,* 1986; *Verhoeven,* 1993], and they can be classified into three main categories:

- Fourier transform methods
- Algebraic methods
- Statistical methods

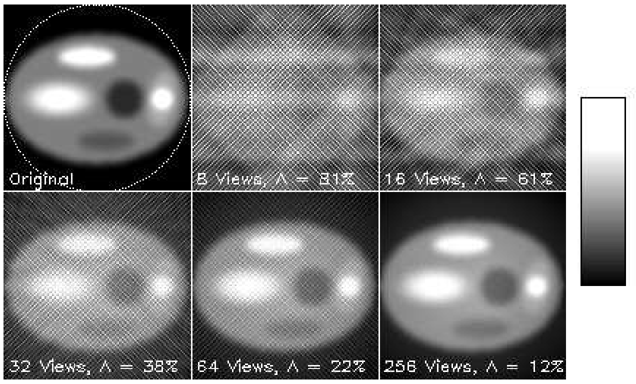

Figure 3. Improvement of the filtered backprojection reconstruction with increasing number of observations. The upper left panel contains the phantom which is used with all methods and shows the circle of observer locations. The relative error Λ in % is indicated.

2.2. Quality parameters for the techniques

Any tomographic technique has to be tested with models in order to establish a quantitative criterion for the quality of reconstruction. The correlation coefficient is only a qualitative measure how well the model and the reconstruction vary jointly, but is does not represent the quantitative agreement.

Adapted from medical investigations [*Shepp and Logan,* 1974], a phantom is used which might resemble density structures in a magnetospheric plane with regions of lower and higher electron density than the surrounding area (Figure 3).

In any practical case only the observations (line integrals) are known quantities and any theoretical treatment of the observation process applied to the reconstructed data has to provide good agreement with the measured data after the influence of noise has been taken into account. As the most important goal of tomography is the agreement between the reconstructed $\hat{f}(x,y)$ and the original distribution $f(x,y)$, a quantitative reconstruction parameter Λ_k is defined:

$$\sum_x \sum_y \sqrt{[f(x,y)-\hat{f}(x,y)]^2} = \Lambda_k \cdot \sum_x \sum_y f(x,y). \quad (4)$$

2.3. Fourier transform methods

Fourier transform (FT) techniques use the Fourier Slice Theorem which states that the FT of a projection is equal to the slice through the FT of the original object [*Kak and Slaney,* 1987]. Thus, given FTs $\mathcal{F}(p_i)$ of projections p_i from the complete angular range around the object will provide the original distribution by simple inversion. However, in reality, only a finite number of observations is available. Hence, interpolation between the FTs of the projections in the frequency domain is necessary to obtain the complete FT of the object. Since the FT of the individual projection can be regarded as a filtered FT of the object, this interpolation is mostly done after a weighting of the projection FT in the frequency domain by filtering with a filter function $\tilde{c}$. This leads to the Filtered Back-Projection (FBP) method which is mostly used in medicine [*Kak and Slaney,* 1988]

$$\hat{f} = \sum_i b_{i\theta t}^{xy} \, \mathcal{F}^{-1}\left[\tilde{c}\mathcal{F}(p_i)\right] \quad (5)$$

The weighting factor $b_{i\theta t}^{xy}$ is the inverse of $h_{xy}^{i\theta t}$ in (2) and establishes the geometrical correspondence between the object and the projection.

Figure 3 shows how the quality of the FBP reconstruction improves with an increasing number of equally separated observations. In this investigation FBP is the only method used with parallel beams.

2.4. Algebraic methods

Direct inversion methods have only limited use in geophysical inverse problems. The matrices involved are often ill-conditioned and so direct matrix inversion is not possible. Inversion by singular value decomposition handles many problems associated with ill-conditioning but is far too computationally intensive for the large dimensions encountered in many real geophysical data sets.

Algebraic reconstruction techniques (ART) solve the problem in an iterative scheme. Several types of ART differ in the way the corrective term is determined while the iteration is always performed on a ray by ray basis until the calculated projection $p_{i,l(\theta,t)}^k$ of the iteration k is as close as possible to the measured data $p_{i,l(\theta,t)}^e$ [*Gilbert,* 1972].

Mainly, we distinguish three types:
additive ART (ART) with the non-negative constraint

$$\hat{f}^{k+1}(x,y) = \hat{f}^k(x,y) + b_{i\theta t}^{xy}\left(p_{i,l(\theta,t)}^e - p_{i,l(\theta,t)}^k\right) \quad \geq 0 \quad (6)$$

multiplicative ART (MART)

$$\hat{f}^{k+1}(x,y) = \hat{f}^k(x,y) \cdot b_{i\theta t}^{xy} \, \frac{p_{i,l(\theta,t)}^e}{p_{i,l(\theta,t)}^k} \quad (7)$$

simultaneous iterative ART (SIRT)

$$\hat{f}^{k+1}(x,y) = \hat{f}^k(x,y) \cdot \frac{1}{I} \sum_i b_{i\theta t}^{xy} \, \frac{p_{i,l(\theta,t)}^e}{p_{i,l(\theta,t)}^k} \quad (8)$$

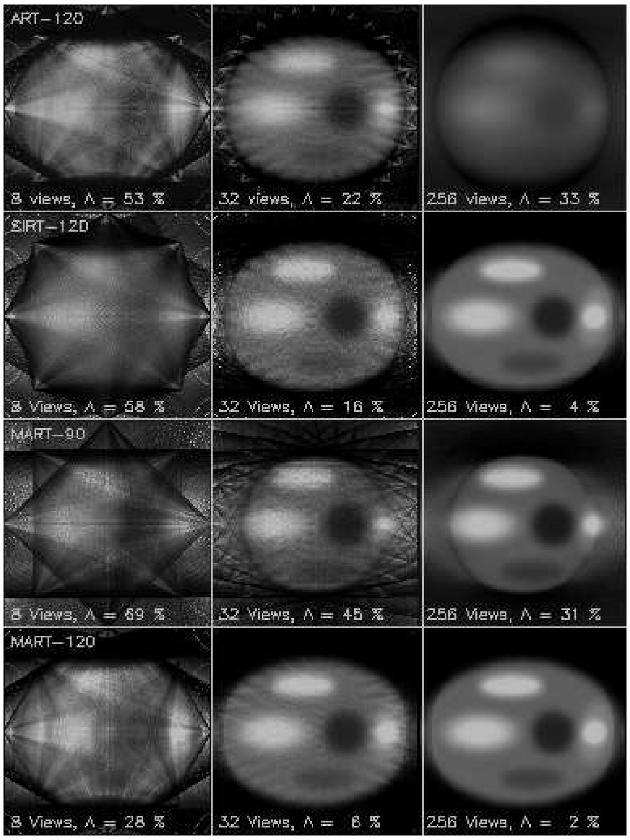

Figure 4. Reconstructions of the phantom by algebraic methods from 8, 32, and 256 views, respectively with fields of view of 90° and 120°.

All methods use back-projection (BP) [*Budinger and Gullberg,* 1974] which projects and sums each projection to the object space filling each line with the data of the projection [*Peyrin,* 1985]

$$\hat{f}(x,y) = \frac{T}{T'} \cdot \sum_{i,\theta,t} b_{i\theta t}^{xy}\ p_i(\theta,t) \tag{9}$$

with establishing the quantitative correspondence with the density T of the element and the density T' of the complete array. This method is very fast but the many simplifications generally return too high cell contents.

The iterations generally start with a homogeneous first estimate. Its selection is of main importance for the applicability of a method and for the number of iterations. In a modification of the MART *Frey et al.,* [1996] reconstruct the first estimate from the BP of projections

$$\hat{f}(x,y) = \min_i \{b_{i\theta t}^{xy}\ p_i(\theta,t)\} \tag{10}$$

where each element is assigned the minimum of the back-projected data. This modification provides the advantage that a cell content once set to 0 cannot increase.

Figure 4 shows reconstructions with ART, SIRT, and modified MART with 90° and 120° field of view. For the given geometry the object is bigger than the region seen with the 90° field of view. This makes the inversion less accurate than in the case of 120° field of view, when the outer border of the object is recognized.

MART has successfully been used for the 3D reconstruction of the volume emission in an auroral arc [*Frey et al.,* 1996a]. The good correspondence between the reconstructed volume emission and the electron density measured by the EISCAT radar was later used to cross-calibrate the volume emission and to calculate the ionospheric conductivity [*Frey et al.,* 1998]. This large-scale conductivity distribution together with the radar measured electric field can then be used to determine ionospheric properties in and outside an auroral arc.

If the original image is known to be reasonably smooth then a least squares (LS) method can be used. This method assumes the original image can be represented by a smooth function of two independent variables and some large number of parameters. Typically these parameters could be the value of the function at fixed locations and the function would perform a 2-D interpolation between these points. Here we use the function:

$$\hat{f}(x,y) = C_0 + C_1 x + C_2 y + \sum_{n=3} C_n D_n ln D_n \tag{11}$$

$$D_n = \sqrt{(x - X_n)^2 + (y - Y_n)^2}$$

where (X_n, Y_n) are the coordinates of the fixed points and C_n are adjustable parameters. These points need not to be on a regular grid. As the line integrals p_i then become linear functions of the parameters C_n, standard linear least squares analysis can be used to determine the values of the C_n which best fit the measured values of p_i. Figure 5 shows results from 16 and 32 observations, and the resolution in this case can not be better than the distance between the grid points.

Alternatively, the density n(x,y) can be equated to the exponential of $\hat{f}(x,y)$, i.e. $n = exp(\hat{f})$. Although non-linear least squares analysis is then required, this has the benefit of forcing the density to be positive definite.

The natural pixel (NP) object representation was developed for tomography from incomplete data and irregularly viewing geometries [*Buonocore et al.,* 1981], and has recently been applied to the problem of ionospheric radio tomography [*Semeter and Kamalabadi,* 1998]. In NP tomography, the object is represented by a basis expansion. Consider a set of tomographic measurements

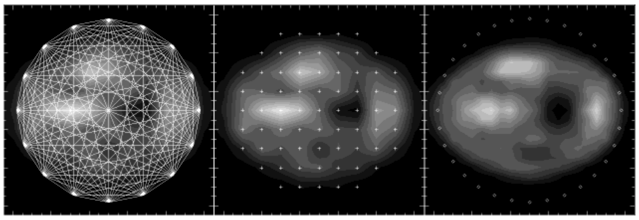

Figure 5. Reconstructions from a least squares method. 120 lines connect 16 observation points and each line represents one line integral (left). The reconstructed image shows the location of fixed points (X_n, Y_n) (center). The reconstruction from 32 observations is shown to the right.

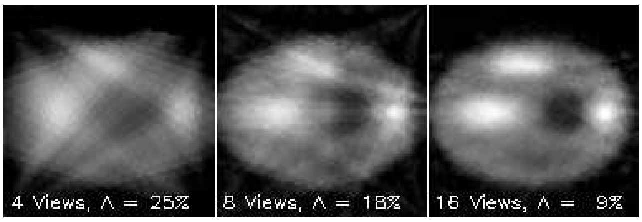

Figure 6. Reconstructions of the phantom from natural pixel presentation. Each equally-spaced projection uses 32 equally-spaced rays.

through a region of interest Ω containing $f(x, y)$. A natural pixel is a characteristic function with the following definition:

$$\phi_i(x,y) = \begin{cases} 1 & \text{(x,y) lies in field-of-view of measurement } i \\ 0 & \text{otherwise} \end{cases} \tag{12}$$

The measurement p_i is specified by

$$p_i = \int_\Omega f(x,y)\phi_i(x,y)dxdy \tag{13}$$

Now assume that $\hat{f}(x, y)$ is adequately represented by a linear combination in this basis, i.e.,

$$\hat{f}(x,y) = \sum_j q_j \cdot \phi_j(x,y) \tag{14}$$

where the q_j are the coefficients of the NP expansion. Substituting (14) into (13) we have

$$p_i = \sum_j q_j \underbrace{\int_\Omega \phi_j(x,y)\phi_i(x,y)dxdy}_{C_{ij}} \tag{15}$$

The term c_{ij} is the inner product of natural pixel i with natural pixel j. These form the elements of the NP projection matrix C whose elements are the areas of polygons defined by overlapping ray boundaries. Tomographic reconstruction involves solving the matrix equation $p = Cq$ [*Buonocore et al.,* 1981]. The coefficients q are then backprojected into a displayable grid. Fig. 6 shows an example of NP-reconstruction. Note that useful features are reconstructed with only 4 projections, but that the results are generally worse than MART as the number of views increases.

In principle, NP offers many advantages over other techniques for image reconstruction from incomplete data. Useful results are achieved at low computational overhead and are devoid of many of the incomplete data artifacts present in other techniques. The NP-representation leads to a framework by which scale-dependent features in the data can be related to scale-dependent features in $f(x, y)$ [*Bhatia et al.,* 1997].

However, there are also significant drawbacks to the NP representation. The matrix C is full and individual projections cannot be processed separately. Thus tremendous storage is required for large problems. There is also no direct way to impose solution positivity, although *Semeter and Kamalabadi* [1998] have recently proposed a technique for refining NP reconstructions under a positivity constraint.

2.5. Statistical methods

Statistical methods consider the measurements as a stochastic process and look for the most probable solution. They mostly use Maximum Likelihood (ML) methods which reconstruct the original distribution in an iteration process as [*Shepp and Vardi,* 1982]

$$\hat{f}^{k+1}(x,y) = \hat{f}^k(x,y) \sum_i \frac{p_i(\theta,t)c_{xi}}{\sum\limits_{n=1}^{N} c_{ni}\hat{f}^k(x,y)} \tag{16}$$

with the probability c_{xi} of detection of an emission event in pixel x in the projection i.

The ML has successfully been used in positron emission tomography and the main advantage is the solid theoretical basis, the good convergence, and the robustness against statistical noise [*Shepp and Vardi,* 1982].

Stochastic inversion (SI) has been used in reconstructing the F region electron density from difference Doppler measurements of total electron content, obtained from navigation satellites and a chain of ground-based receivers [*Nygrén et al.,* 1996]. The results have been compared to simultaneous electron density measurements carried out by the EISCAT incoherent scatter radar.

In this method all measurements are collected into a

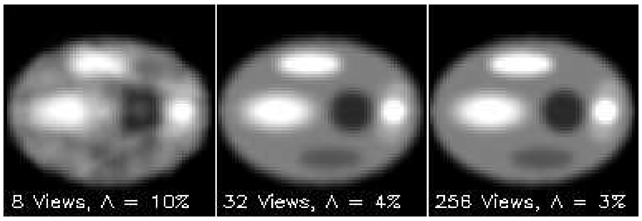

Figure 7. Results of stochastic inversion.

single column vector $\mathbf{p}$, their errors into a column vector ϵ_p, and the unknowns into a column vector $\mathbf{f}$ with $\mathbf{p} = \mathbf{A_p} \cdot \mathbf{f} + \epsilon_\mathbf{p}$, where $\mathbf{A_p}$ is a matrix of linear coefficients. Similarly, writing an equation $0 = f_n - f_m + \varepsilon_r^{(nm)}$ for the unknowns f_n and f_m at each pair (n, m) of neighbouring grid points gives a matrix equation $\mathbf{0} = \mathbf{A_r} \cdot \mathbf{f} + \epsilon_\mathbf{r}$. Here the components of $\epsilon_\mathbf{r}$ are the errors made when the differences $f_n - f_m$ are put to zero. Both $\mathbf{p}$, ϵ_p, $\mathbf{f}$, and ϵ_r are treated as random variables. Assuming that the distributions of ϵ_p and ϵ_r are Gaussian with covariance matrices $\mathbf{\Sigma_p} = \langle \epsilon_\mathbf{p} \cdot \epsilon_\mathbf{p}^\mathbf{T} \rangle$ and $\mathbf{\Sigma_r} = \langle \epsilon_\mathbf{r} \cdot \epsilon_\mathbf{r}^\mathbf{T} \rangle$, respectively, and the mean value $\langle \epsilon_\mathbf{r} \rangle = \mathbf{0}$, the conditional density of the unknowns is [*Nygrén et al.,* 1997]

$$D(\mathbf{f}|\mathbf{p}, \mathbf{0}) \propto D_{pr}(\mathbf{f}) \cdot \exp\left[-\frac{1}{2}(\mathbf{A_r} \cdot \mathbf{f})^T \cdot \mathbf{\Sigma_r^{-1}} \cdot (\mathbf{A_r} \cdot \mathbf{f})\right]$$

$$\cdot \exp\left[-\frac{1}{2}(\mathbf{A_p} \cdot \mathbf{f} - \mathbf{p})^T \cdot \mathbf{\Sigma_p^{-1}} \cdot (\mathbf{A_p} \cdot \mathbf{f} - \mathbf{p})\right] \qquad (17)$$

Here T indicates the transpose. The inversion solution is obtained as a maximum point of the conditional density $D(\mathbf{f}|\mathbf{p}, \mathbf{0})$ or as the mean value of $\mathbf{f}$. If no a priori information is used, these solutions are identical. Then the inversion problem is linear, and the maximum likelihood point is simply given by

$$\hat{\mathbf{f}} = (\mathbf{A_p}^T \cdot \mathbf{\Sigma_p^{-1}} \cdot \mathbf{A_p} + \mathbf{A_r}^\mathbf{T} \cdot \mathbf{\Sigma_r^{-1}} \cdot \mathbf{A_r})^{-1} \mathbf{A_p}^\mathbf{T} \cdot \mathbf{\Sigma_p^{-1}} \cdot \mathbf{p} \quad (18)$$

Here $\mathbf{A_r}^T \cdot \mathbf{\Sigma_r^{-1}} \cdot \mathbf{A_r}$ is a non-diagonal regularization matrix which stabilizes the solution. A smoothly behaving solution is obtained by means of a proper choice of the covariance matrix $\mathbf{\Sigma_r}$.

If the unknown function cannot have negative values, the non-negativity constraint can be implemented by means of an a priori density $D_{pr}(\mathbf{f})$, which makes the inversion problem nonlinear. Then, instead of (18), it is possible to search for a set of random vectors $\hat{\mathbf{f}}$ obeying the posteriori distribution in (17). This can be done by means of Gibbs sampling. When the set is large enough, the average of the sample vectors gives a good estimate to the statistical average of $\hat{\mathbf{f}}$. In this case the average is given as the inversion result instead of the maximum likelihood point (Figure 7).

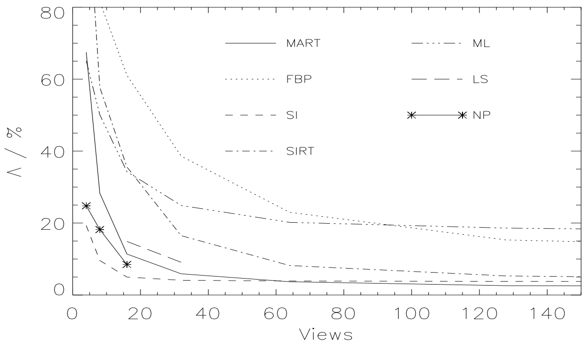

Figure 8. Mean error of methods for an increasing number of observers around the phantom.

3. Results of the methods

For tests of the reconstruction methods observations of the phantom from 4 to 256 directions were simulated. The accuracy of tomography may be improved by the introduction of a-priori knowledge about the object like smoothness, the extent, or the non-negativity. For algebraic and statistical techniques it is generally easy to incorporate this knowledge to limit the number of possible solutions, or speed-up the iteration [*Trussel,* 1984]. FT techniques can generally not include this information.

If an object is to be uniformly resolved to a resolution d, the number of discrete views must be at least

$$n \approx \pi D/d \qquad (19)$$

with the dimension of the object D [*Budinger and Gullberg,* 1974]. With our phantom at least 25 equally separated views are necessary to resolve the smaller structures.

For this example the MART and SI yield the best results (Figure 8). While the SI reached errors $< 10\%$ with as low as 8 observations, the MART got better results than SI with more than 64 observations.

The difference between the methods is that all used 128 rays from each observer except the LS with only (n-1) rays and NP with 32 rays. This limited the total number of useful rays for LS to n(n-1)/2 and from the corresponding small number of grid points, the results of this method for 16-32 observers are quite good.

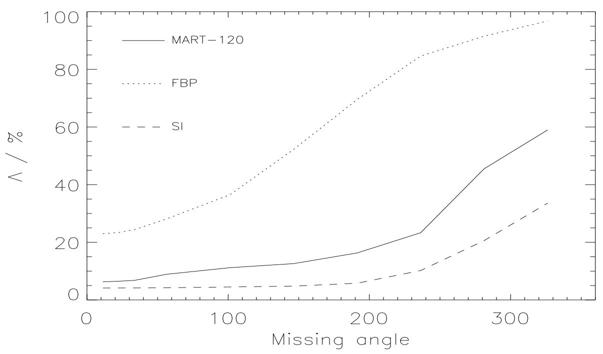

Figure 9. Quality parameter Λ for a reconstruction with a missing cone in the observation directions starting with 32 equally spaced observers around the phantom. FBP has been adjusted to the parallel beam geometry.

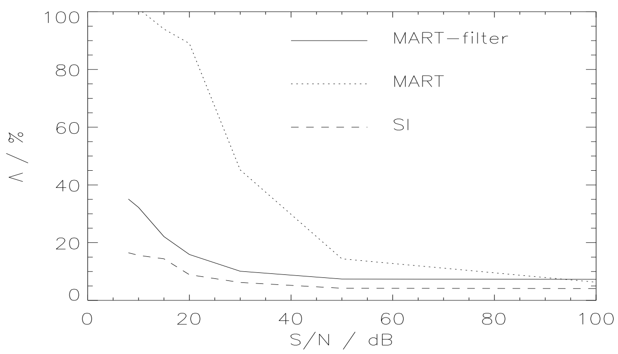

Figure 10. Effect of noise on the reconstruction parameter.

The problem with all methods is that there is no confirmed mathematical or physical reason to set particular pixel elements to zero, except for the modified MART where this is done at least for all the pixels along a ray from one of the observers which showed zero content in the image. Because the total intensity within the images has to correspond to the total source distribution, some pixels at the outer surface of the object contain intensity which is then missing in the center pixels. This is also most probably the reason why radio tomography tends to overestimate the electron density on the topside of the reconstruction [*Walker et al.,* 1996] and to produce thicker layers [*Nygrén et al.,* 1996].

Comparing the results in Figure 8 it has to be kept in mind, that all methods used iterations (up to 64) in order to obtain the small resulting errors, except the FBP and SI, which only used one reconstruction. The FBP is a good method if many observations from the full angular range are available and if no iterations are used. Since this is the exception rather than the rule in geophysical applications, use of this method is limited.

The SIRT is a good method if many observations are available, because in this case the mean values in the update scheme produce sufficient effects. While ART and SIRT encounter problems in determining the areas with lower density than the surrounding, the modified MART can at least determine the circular area of our phantom. The iterations provide an opportunity to recover sufficient reconstructions already from 16 observations (23° separation). However, as predicted by Equation (19) a minimum number of 32 observations ($\approx 12°$ separation) was necessary for most methods to achieve a satisfactory quantitative reconstruction of the phantom (Figure 8).

The algebraic and statistical methods are more robust against missing cones than the FBP. This is shown in Figure 9, where the mean error is given for 32 equally separated observations and a missing cone region from $\theta = 0°$ to $\theta = \theta_1$. The agreement between the original phantom and the reconstruction is best for the SI. It provides the best reconstruction of the overall shape of the object. The agreement is still sufficient for the modified MART as long as the missing cone does not reach more than 200°.

Noise always deteriorates the quality of real images. As a quantitative test noise was added to the projections with increasing noise and decreasing signal-to-noise ratio S/N [*Verhoeven,* 1993]

$$S/N = 10 \log \left(\sum_i p_i^2 / \sum_i \Delta p_i^2 \right) \qquad (20)$$

where Δp_i is the ray sum error caused by the noise (Figure 10). The SI is very robust against noise and can handle S/N values down to 10 dB. Without noise reduction the results of the MART get already much worse at signal to noise ratios of less than 50. The non-negative constraint improves the situation, but the median filter best improves to acceptable signal to noise ratios greater than 20. In this way some knowledge about the nature of noise sources may help to improve MART results by proper filtering.

4. Conclusions

The goal of this paper was to compare different tomographic reconstruction methods to find those which might work best for a magnetospheric radio-tomography mission with the limitations of a small number and probably a limited angular range of observations. The phantom which was used for this investigation contained not only regions with higher density than the surrounding, but also regions with lower density.

Overall the best results were obtained with the SI, not only for a small number of observers, but also in view of missing cones and the robustness against noise. The method is computationally quite extensive, however still very fast with about 10 minutes calculation time because it does not use iterations.

The second best methods are the modified MART, NP and LS. MART provides very good reconstructions with more than 32 observers, tolerates large missing cones, and can adjust noise after preprocessing. The LS and NP yield good results for a small number of observers.

The FBP, ML, and SIRT methods have bigger problems with the reconstruction quality and might not be very well suited for magnetospheric applications.

This investigation was performed for magnetospheric satellite radio tomography. For the purpose of ionospheric satellite radio tomography, the value of the comparisons made in this paper is limited by the fact that, in that case there is always a large sector around the horizontal direction with no observations. These missing observations would contain information on the vertical ionospheric profile, and the absence of this information poses the main problem in satellite radio tomography.

Acknowledgment. We are grateful to M. Markkanen for carrying out the SI calculations. Support from the Academy of Finland is acknowledged by T.N.

References

Aso, T., T. Hashimoto, M. Abe, T. Ono, and M. Ejiri, On the analysis of aurora stereo observations, *J. Geomagn. Geoelectr., 42,* 579–595, 1990.

Bhatia, M., W. C. Karl, and A. S. Willsky, Tomographic reconstruction and estimation based on multiscale natural-pixel bases, *IEEE Trans. Image Proc., 6,* 463, 1997.

Budinger, T. F., and G. T. Gullberg, Three-dimensional reconstruction in nuclear medicine emission imaging, *IEEE Trans. Nucl. Sci., NS-21*, 2–20, 1974.

Buonocore, M. H., W. R. Brody, and A. Macovski, A natural pixel decomposition for two dimensional image reconstruction, *IEEE Trans. Biomed. Eng., BME-28,* pp. 69-78, 1981.

Doe, R. A., J. D. Kelly, J. L. Semeter, and D. P. Steele, Tomographic reconstruction of 630.0 nm emission structure for a polar cap arc, *Geophys. Res. Lett., 24,* 1119-1122, 1997.

Frey, S., H. U. Frey, D. J. Carr, O. H. Bauer, and G. Haerendel, Auroral emission profiles extracted from three-dimensional reconstructed arcs, *J. Geophys. Res., 101,* 21731–21741, 1996a.

Frey, H. U., S. Frey, B. S. Lanchester, and M. Kosch, Optical tomography of the aurora and EISCAT, in press in *Ann. Geophys.*, 1998.

Gilbert, P., Iterative methods for the three dimensional reconstruction of an object from projections, *J. Theor. Biol., 36,* 105–117, 1972.

Hayner, D. A. and W. K. Jenkins, The missing cone problem in computer tomography, in *Advances in Computer Vision and Image Processing,* JAI Press, Tokyo, 1984.

Kak, A. C. and M. Slaney, *Principles of Computerized Tomographic Imaging*, IEEE Press, New York, 1988.

Menke, W., *Geophysical data analysis: Discrete inverse theory,* Academic Press, Inc., New York, 1984.

Natterer, F., *The Mathematics of Computerized Tomography*, John Wiley, New York, 1986.

Nygrén, T., M. Markkanen, M. Lehtinen, E. D. Tereshchenko, B. Z. Khudukon, O. V. Evstafiev, and P. Pollari, Comparison of F-region electron density observations by satellite radio tomography and incoherent scatter methods, *Ann. Geophys., 14,* 1422–1428, 1996.

Nygrén, T., M. Markkanen, M. Lehtinen, E. D. Tereshchenko and B. Z. Khudukon, Stochastic inversion in ionospheric radiotomography, *Radio Sci., 32,* 2359-2372, 1997.

Peyrin, F. C., The generalized back projection theorem for cone beam reconstruction, *IEEE Trans. Nucl. Sci., 32*, 1512–1519, 1985.

Raymund, T. D. S. J. Franke, and K. C. Yeh, Ionospheric tomography: its limitations and reconstruction methods, *J. Atmos. Terr. Phys., 56,* 637–657, 1994.

Semeter, J. and F. Kamalabadi, A natural pixel decomposition for tomographic imaging of the ionosphere, *Proc. Int. Conf. Acoustics, Speech and Signal Processing (ICASSP)*, Seattle, Washington, 1998.

Shepp, L. A. and B. F. Logan, The Fourier reconstruction of a head section, *IEEE Trans. Nucl. Sci., NS-21,* 21–43, 1974.

Shepp, L. A. and Y. Vardi, Maximum likelihood reconstruction for emission tomography, *IEEE Trans. Med. Imaging, 1,* 113–122, 1982.

Trussel, H. J., A priori knowledge in algebraic reconstruction methods, in *Advances in computer vision and image processing,* JAI Press Inc., 1984.

Vallance Jones, A., et al., Characterization and modeling of an evening auroral arc observed from a rocket and a ground-based line of meridian scanners, *Planet. Space Sci., 39,* 1677–1705, 1991.

Verhoeven, D., Limited-data computed tomography algorithms for the physical sciences, *Appl. Optics, 32,* 3736–3754, 1993.

Walker, I. K., J. A. T. Heaton, L. Kersley, C. N. Mitchell, S. E. Pryse, and M. J. Williams, EISCAT verification in the development of ionospheric tomography, *Ann. Geophys., 14,* 1413–1421, 1996.

H. U. Frey, S. Frey, D. Larson, Space Sciences Laboratory, University of California, Berkeley, CA 94720-7450, email: hfrey@ssl.berkeley.edu.

T. Nygrén, Department of Physical Sciences, University of Oulu, FIN-90570 Oulu, Finland

J. Semeter, Max-Planck-Institute for Extraterrestrial Physics, D-85740 Garching, Germany

---

This preprint was prepared with AGU's LaTeX macros v4, with the extension package 'AGU^{++}' by P. W. Daly, version from .